Analysis of Focal-Plane Measurements for VERITAS Telescopes

William Hemmo Schuur

In this experiment we measured the Point Spread Function (PSF) of the telescope at different image locations using a python GUI and servo motors to automate a screen along the focal axis of the telescope. Our results show that the telescope T4 has a well-defined image distance at each elevation, but this distance shifts as the telescope is lowered. Additionally, off-axis telescope orientations are degraded by aberrations and at low elevation possibly some structural warping of the mirror. The VERITAS Telescopes are located in Southern Arizona at the Fred Lawrence Whipple Observatory.

June 2012

Cal Poly San Luis Obispo

Contents

1 – Introduction to the Science of VERITAS

Finished in 2007, the Very Energetic Radiation Imaging Telescope Array System (VERITAS) is a 4 telescope array located in southern Arizona. VERITAS is funded by the U.S. Department of Energy, the National Science Foundation, Smithsonian Institution, the Natural Sciences and Engineering Research Council (NSERC) in Canada, Science Foundation Ireland and the Science and Technology Funding Council (STFC) in the United Kingdom. The VERITAS collaboration focuses their efforts on mapping the night's sky in an attempt to understand black holes and other exotic phenomena.

Distant stars spiral around Black holes and at small radii break down into a disk of highly energetic material. These spirals are called accretion disks. From these accretion disks jets of high energy photons are directed out along the rotational axis. The photons that eventually make it to the earth's surface are at energies far too high to be perceived by the naked eye. VERITAS is designed to detect these photons after they've completed their long journey to us on earth. This journey is most interesting once photons reach the earth's atmosphere where they collide with atoms in the air, resulting in an air shower.

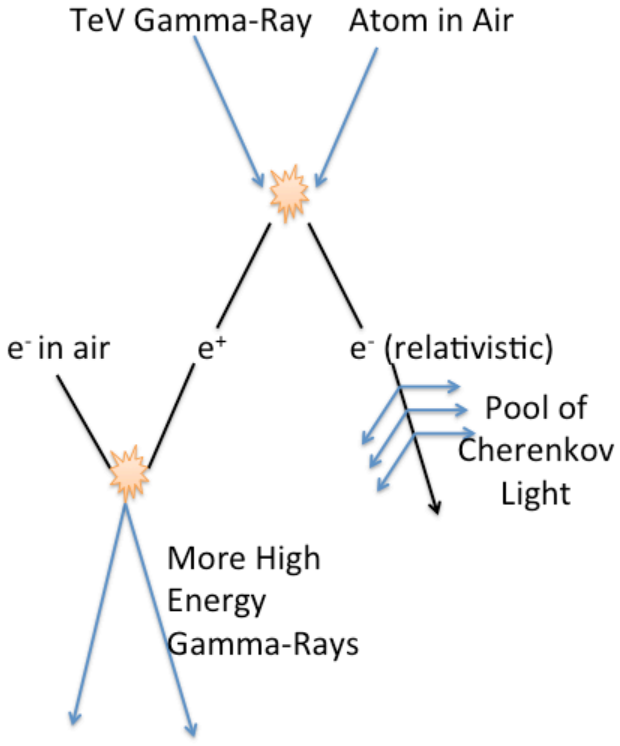

Figure 1 - Pair Production Diagram

A simplified version of an air shower is shown in Figure 1. The high-energy photons go through a process of pair production. This is a process in which a photon's interaction with an atom produces both an electron and positron. As the electrons and positrons move at relativistic speeds through the air they emit photons called Cherenkov photons. The positron collides with an electron in the air resulting in annihilation emitting two more photons, each of which continue the process from the beginning. As the chain reaction continues, the successive photons of decreasing energy are produced. The cascades of electrons and photons created in this manner are called Electromagnetic Showers. Eventually the Cherenkov photons spread into a pool of coherent light at the ground coming from a direction 1° from the original point of entry to the atmosphere. The Cherenkov photons that reach the ground are ultraviolet.

Figure 2 shows how the VERITAS mirrors reflect the photons toward the camera box. The VERITAS team maps the sky and locates the gamma-ray emitters like the black holes mentioned previously. The 4 telescopes are all outfitted with a honeycomb shaped cluster of Photo Multiplier Tubes (PMTs) to detect the Cherenkov photons. PMTs are commonly used in lab settings, to detect radiation from a source. This application is the basis of all data analysis at the telescopes.

The round PMTs that make up the camera don't fit snugly together, so a set of hexagonal light cones designed to reflect the light into a specific PMT is placed in front of them. That is, if a photon was going to land between two PMTs, it is reflected toward one of them instead. This process makes sure that no photons escape detection by slipping between the gaps in the PMTs.

The camera has a 4° circular field of view that is shown in Figure 3. An image of an air shower is represented by an elevated count rate shown as red and a low count rate is shown as blue. In the figure, the elongated axis of the elliptical "blob" of counts depicts the spread of the pool of Cherenkov light from top to bottom caused by the aforementioned pair productions within the air shower. The shortened axis is a measure of resolution widely known as the Point Spread Function or PSF.

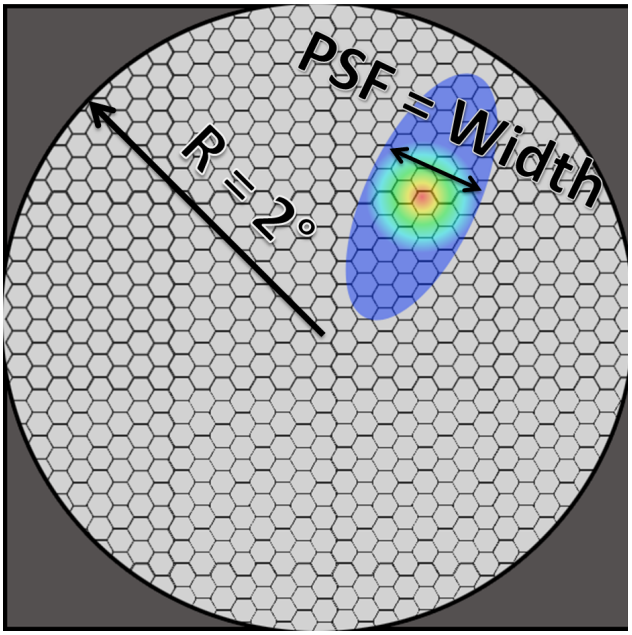

Figure 3 - Graphical PSF Representation

2 - The PSF

2.1 - Definition

The focal length of a reflector is related to the image and object distances by

$$\frac{1}{focal\ length} = \frac{1}{object\ dist.} + \frac{1}{image\ dist.} \qquad (1)$$

which relates the distance a screen should be from a mirror to the specific focal length of the mirror and the distance an object is from the mirror. In the case of sources like air showers, the Cherenkov light comes in as parallel beams, which correspond to object distances of infinity. This result reduces the equation to simply state that the focal length and the image distance are equal.

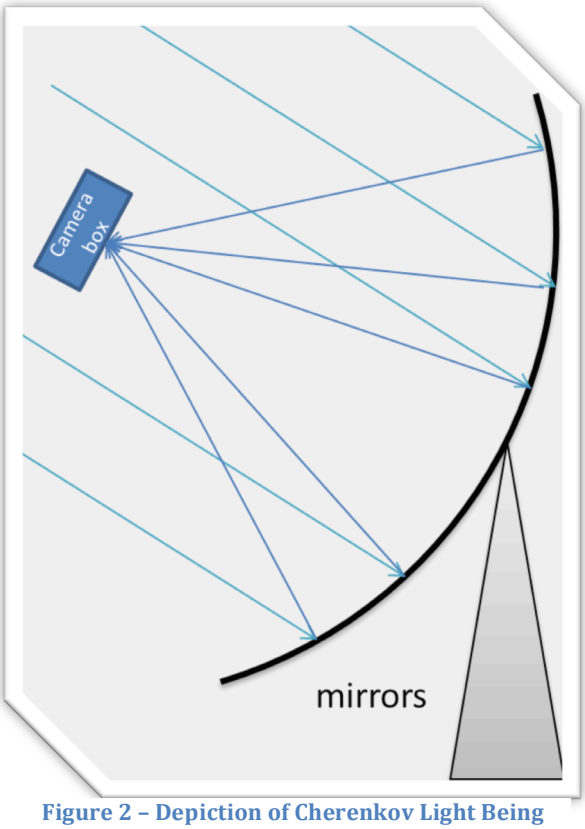

Figure 2 – Depiction of Cherenkov Light Being Reflected into the Camera Box

When this image distance is equal to the focal length, the image on the screen is focused and any blurring is the resolution of the system. In terms of VERITAS, this smallest possible width is the ideal PSF and provides the highest resolution for the telescope.

2.2 - PSF Calibration Procedure

PSF measurements are one of several calibration tests performed annually on the telescope before observing begins in September. Prior to Summer 2011 the hardware didn't allow observers to change the image distance when doing a PSF calibration. The PSF was characterized at a fixed focal plane position. Taking data simply required swapping the light cones with a white screen that was bolted in place.

During normal PSF calibrations, the user typically has two programs running. One is the telescope positioning program which uses a tracking algorithm to follow the source in the sky. The second of these programs controls the VERITAS

Pointing Monitor (VPM) camera that takes pictures of the light on the PSF screen and saves them to a SQL database for later analysis by a program called Plotpsf.

This procedure ignored the issue of characterizing the PSF at varying image distances. Attempts had been made to adjust the image distance by hand, but this method proved so tedious and time consuming that the effects of focal length were never fully examined.

3 - The Servo Automation Method

3.1 – Hardware & Software Development

We improved the procedure by mounting the white screen on servo motors to move the screen along the Z-axis. The Z-axis is labeled in Figure 4. As the Z value is varied, the image distance is changed with it.

As illustrated in Figure 5, a large number of components went into controlling the servos effectively. We purchased three Firgelli L16-150-100-12-P servo motors each controlled by its own Firgelli Linear Actuator Control Board (LAC). To control 3 servos at the same time a Phidgets Servo Controller was purchased. The Controller sends signals via a 3-pin RC connector which contains ground, control voltage and power leads to the LAC. These inputs are interpreted by the LAC and converted to a 5-pin potentiometer signal that controls the extension and retraction of the servos. As we show in this report, the convenience of having the screen automated allowed a full characterization of the PSF from data collected in a single night.

A python Graphical User Interface or GUI was developed to control the servos from a computer. However, operating the laptop from the camera platform is inconvenient while the telescope is observing. To alleviate this problem a Plug Computer was purchased. These are small but surprisingly powerful computers about the size of the power adapter found in electronic devices like speakers. They run their own build of Linux. They are small and allow secure shell access (SSH) making them ideal tools for remote control applications.

The GUI was accessed by SSHing into the Plug Computer mounted in the camera box with the USB servo controller box. To properly examine the data, the position of the servos needed to be recorded. This data was saved to the VERITAS SQL database that services all applications on site. We stored the position and time data. Once we had learned the basics of SQL databases, the actual writing of our servo data was simple.

The script designed to write this data operated like a trap. The trap was armed when one or more servos indicated a sufficient increase in current meaning the servo was moving. It was sprung when all the currents had dropped again meaning the servos were stopped. Once the trap was sprung, the script queried all three servos with the get position command and stored the 3 servo positions and the current time to the database for future records and analysis.

New processes should fit seamlessly into the telescope environment. The servo control GUI aimed to do just that. From the same computer where the user opens the first two control programs, they now access the servo controller by

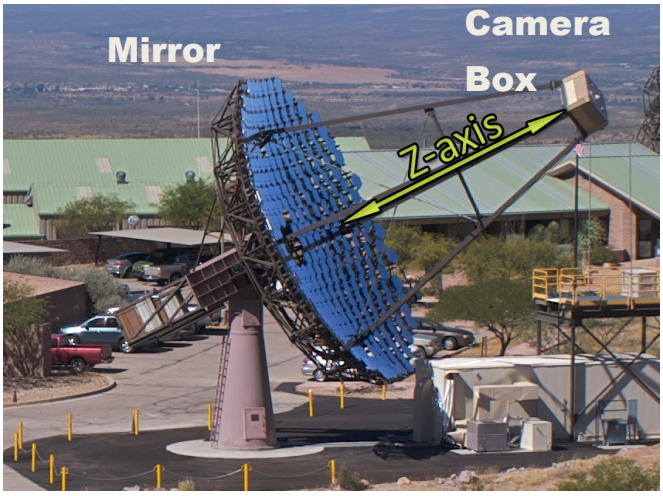

Figure 4 – Telescope T1 at VERITAS Basecamp in the Mountains above Amado, Arizona

SSHing into the Plug Computer. Once logged into the Plug the user runs basic setup bashrc files before running the servo automation GUI shown in Figure 5.

The GUI itself is a python control program. It relied on many functions from the compiled control library provided by the Phidgets company. The majority of these functions are commands for setting position. The servos are given a 0 to 144 setting in servo units (SU), representing full contraction and full extension respectively. This automation sounds simple, but hardware limitations proved to be a problem.

3.2 – Solving Hardware Problems

The servos occasionally stall, not completing their intended path. Since the Phidget controller has no "getActualPosition" from the LAC boards, we had no way to know when a stall had occurred. The "getPosition" command simply passes the most recent "setPosition" value back. This problem was found in early testing prior to adding the additional strain of the screen to the motors and before the 10cm-long motors were angled due to the telescope's elevation, exacerbating the stalling. Sending the servos from 0 SU to 144 SU usually resulted in at least one stopping short. After many trials we concluded that moving the servos short distances was much more reliable and used that technique during data taking.

A workaround was also found using the "get current" command. This command, when used by a script queries the LAC for a current reading in milliamps. It displayed a somewhat obvious trend that the current increased dramatically while the servos were moving. It rises on the order of 10 times its resting current of 40 mA. Modifying the GUI to detect these increases in current allowed us to observe whether the servos were running for the same amount of time.

3.3 - Installation on Telescopes

Automating the servos and designing the interface between hardware and software was done off-site. The next step was to install the hardware out at the Telescopes. The servos were mounted in brackets which we machined on site using various tools in the mechanic's shop.

A ¼" alumalite screen was purchased to be the new screen for the image distance PSF measurements. The decision was made to use alumalite, which is corrugated plastic with aluminum on each side. The benefits of using alumalite were twofold: it does not warp if exposed to the humid weather conditions experienced at basecamp and it is light enough that the servos are expected to move it reliably. The previous screens had a triangular shape designed to match up with the posts extending from a fixed frame located in the camera box. Because our three servos are mounted on the same frame it was decided that the alumalite should maintain as much similarity to its predecessors as possible.

To have the servos extend and retract in their intended way, we designed mounts to tightly secure the base end of the servos to the frame. As shown in Figure 6, a steel bracket was machined for each servo, with two screw holes below the servo and a long, supported plate above where the servo extends through the bracket. The screw holes match up perfectly with threaded holes on the frame in the focal box so that the connection is secure and strong enough to withstand motion at the heights reached by the telescope.

Once the servos were reliably affixed to the camera box the next step was to create a lightweight and reliable way to secure the screen to all three servos. We machined a nylon sleeve shown in Figure 6 with its own washer at the base end. The narrow portion fit through corresponding holes in the screen with the wide portion holding the backside. A metal washer was placed on the front, over the nylon and then a screw ran through the nylon and through a hole in the tip of the servo, which pinched the screen between the nylon and the washer.

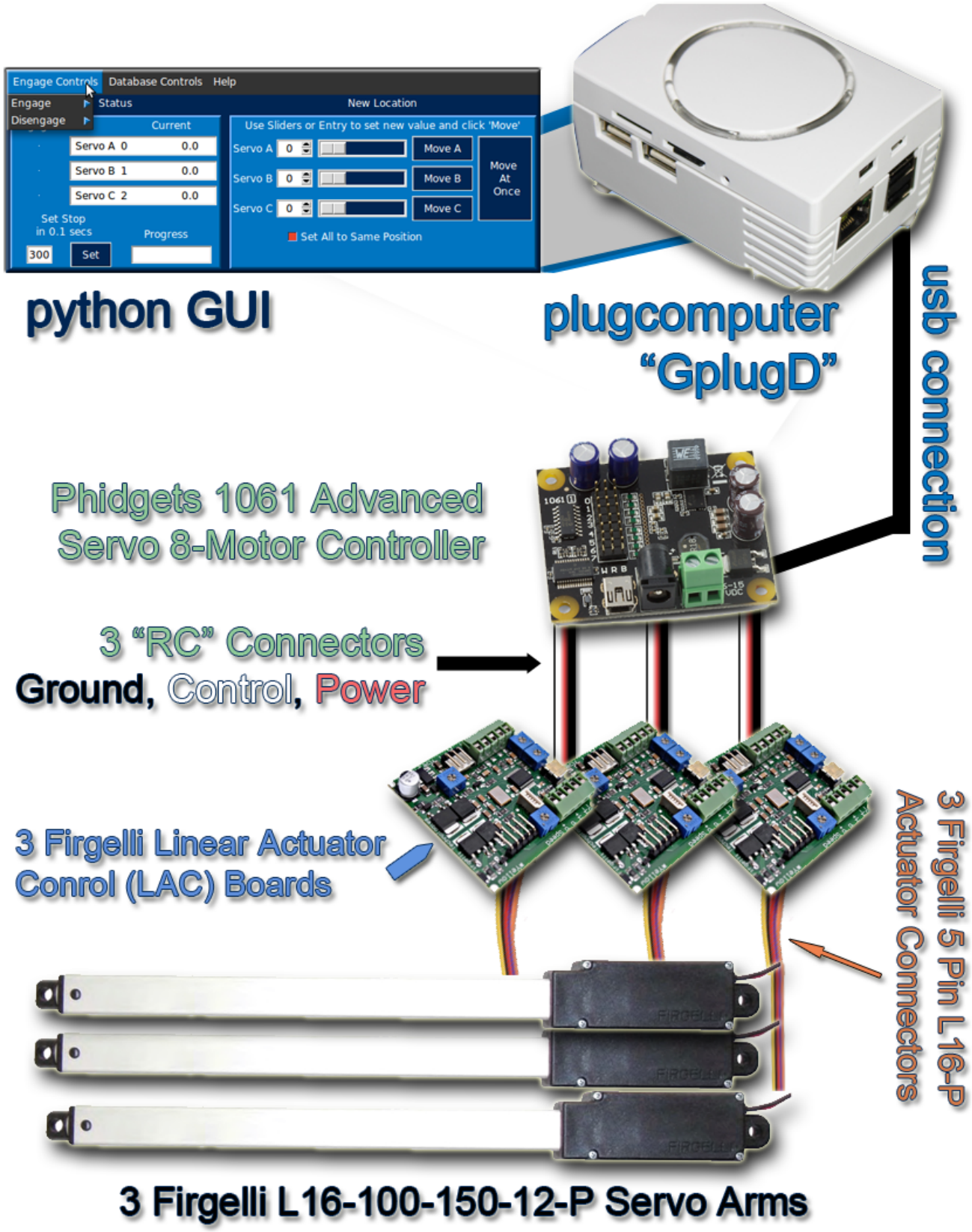

Figure 5 - Graphical Representation of Hardware and Software Interactions

3.4 – Calibration & Raw Data

To convert the servo position reported as a number between 35 SU and 144 SU into a distance from the face of the PMTs in the camera we accounted for both screen thickness and servo extension. After taking measurements of each servo using a micrometer at different positions, we fitted the data to a straight line, and found the calibration equation,

$$Z_{mm} = (0.669 \pm 0.003)\ \frac{mm}{SU}\ Z_{SU} + (1.6 \pm 0.3)mm \quad (2)$$

where Z_{mm} is the position of the screen in mm in front of the PMTs and Z_{SU} is the set position as reported by the servo. This means that our 35-144 SU range corresponds to 7.29±0.10 cm range of extension.

Once the hardware was installed the next step was to take data. Typical PSF data was taken using the VPM camera located halfway along the telescope's camera support beam. The camera saves a FITS file to the VERITAS SQL database. A focused image is plotted as a 2-D y vs. x graph in pixels and a color scale to represent the number of counts at each pixel as shown in Figure 7. The FITS data are later analyzed by the Plotpsf program. It performs a long series of analysis procedures and produces a 3-D Gaussian fit to the image.

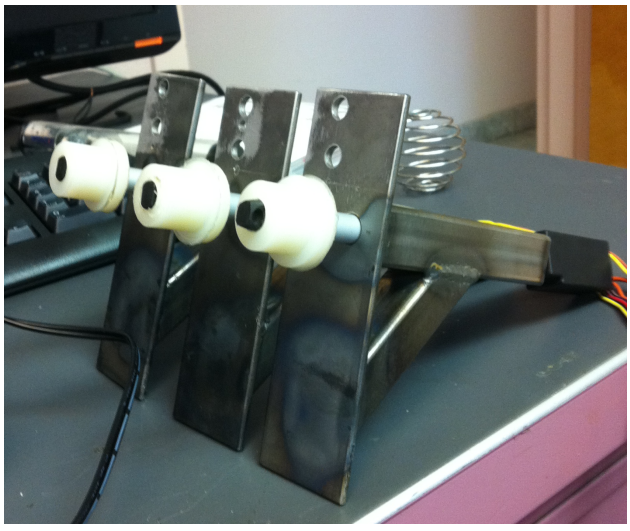

Figure 6 - Hardware Design for Mounting of Servos and Screen

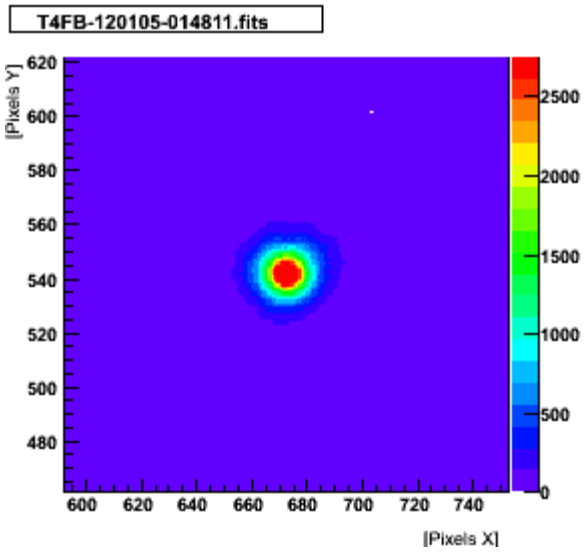

Figure 7 - An Example of the imagef for On-Axis near the focus

4 - The Data Taking Procedure

4.1 - Choice of Measurements

To observe the effects of the image distance on the shape of the PSF, we had to define our independent and dependent variables. There are three independent variables of interest. The primary one is the Z_{SU}, which we modify by moving the servos. The second is the elevation of the telescope. The third is the off-axis location of the camera.

The dependent variable is a bit harder to define. Of the many outputs of Plotpsf program, the most interesting is the aforementioned 3-D Gaussian, known as the "blob". Not only is it the visual representation of the image on the screen, but it also provides a key radius that we chose to use for the remainder of our analysis. The 80% Blob Containment Radius (r_{80}) is the radial distance from the center of the blob to the radius at which 80% of all counts are included. A smaller radius indicates good focus. The smallest 80% containment radius is our best resolution and all larger blobs exhibiting an inflated radius are out of focus.

From basic optics it is known that the rays reflected by a concave reflective surface converge at a point that is called the focal point of the lens or mirror. As a screen moves through the focal point, the image and thus the 80% blob containment radius (r_{80}) on the screen sharpens to a minimum then spreads again.

At the end of the summer we conducted a few basic tests of the procedure. The tests allowed us to better familiarize ourselves with how the GUI and Servos actually perform once installed. Knowing how they actually work allowed future data taking to be more efficient. The mirror facets were not yet aligned so the data itself was inconclusive.

4.2 - January 2012 Data

Martin Schroedter scheduled calibration PSF data taking for January 4th, 2012. He observed five elevations: 32°, 58°, 66°, 78°, 80°. At each of these elevations, Martin picked a star for the telescope to track, moved the servos to six positions: 35 SU, 55 SU, 74 SU, 94 SU, 116, 140 SU and took a VPM picture at each screen position with an exposure time of 200ms. For each elevation and servo position along the z-axis he moved the telescope to 1.2 ° off-axis in the four camera directions; up, down, left and right. The combination of these 5 positions for each Z_{SU} and Elevation is made into a plus-shape for analysis. This plus-shape is shown in Figure 8. The top and bottom off-axis measurements are significant. The left and right monitor stability of the technique.

5 – Analysis & Results

After the FITS files were passed through the Plotpsf program, the 80% blob radius data was put into spreadsheets for further analysis. Elevations 58°

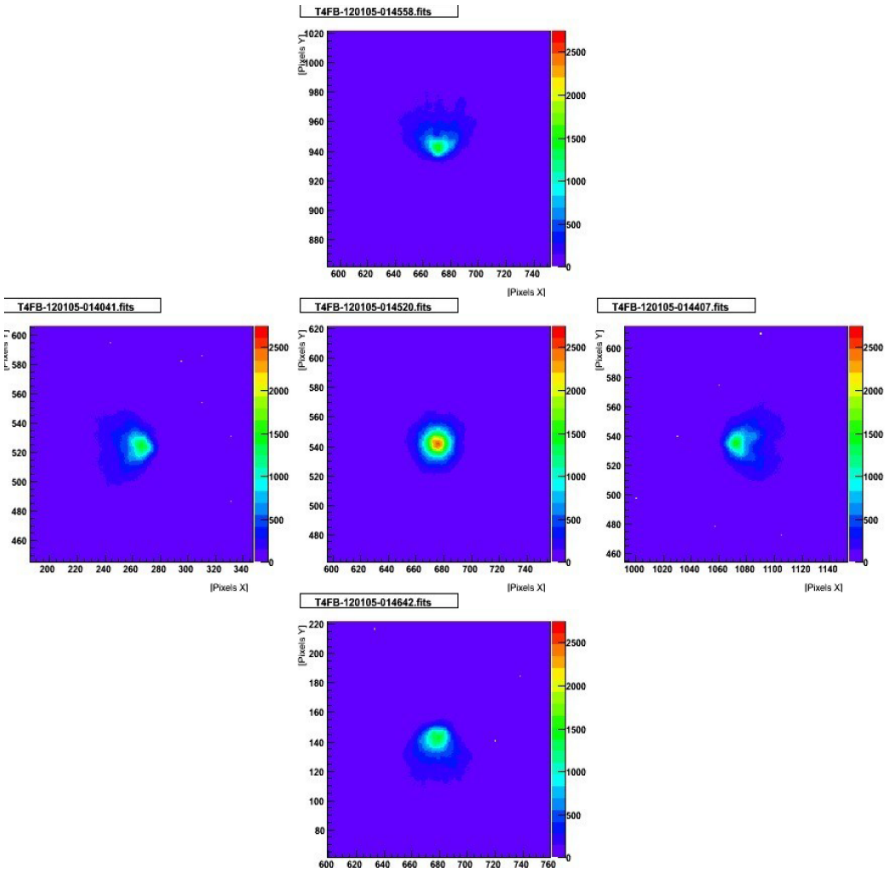

Figure 8 - The Plus-Shape Collection of On and Off Axis Blobs for 66° and Z_{SU} = 35. The center is on-axis. The left, right, top and bottom are taken with the camera pointed 1.2° off-axis from the star imaged here.

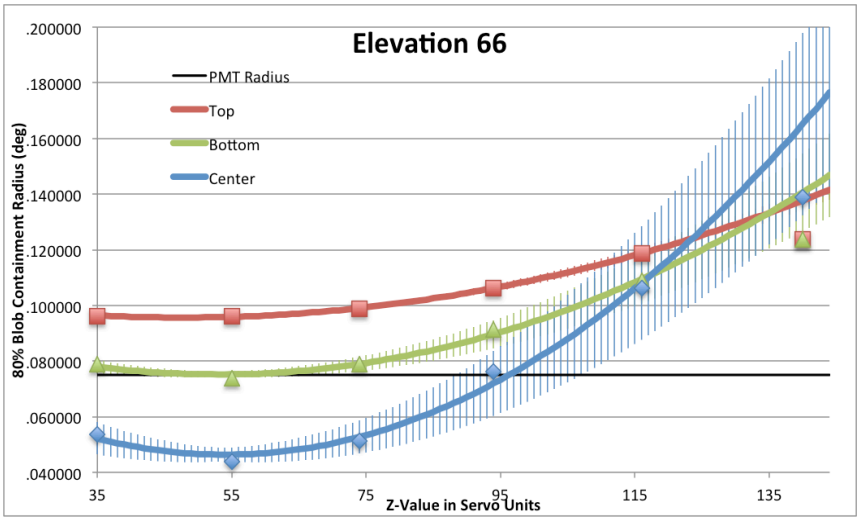

Figure 9 - r_{80} vs. Z_{SU} for Elevation 66°

and 80° were discarded because multiple images at these elevations came out oversaturated or were damaged. Our analysis is based on the elevations of 32°, 66°, and 78°. Most VERITAS science data is collected between 60° and 80°. There is a lot of interest in lower elevation observations too, such as the galactic center. Elevation 32° is near the lowest elevation used in scientific analysis.

The first analysis result is to find the location of the focal planes for each elevation as well as orientation. As the radius shrank and grew with the screen's motion, an expected parabolic shape was measured. The bottom of this parabola indicates the focal length of the telescope. The radius at the bottom is the telescope's measured resolution. These parabolas are shown in r_{80} vs. Z_{SU} plots found in Figures 9-11. Our parabola has the following form,

$$r_{80}(Z_{SU}) = A * (Z_{SU} - B)^2 + C \qquad (3)$$

where A is a coefficient, B is the location of the minimum in Z_{SU} called the focal point and C is the minimum radius, r_{80}. Table 1 has the B and C values organized by orientation and elevation.

Each elevation was analyzed individually. First we looked at elevation 66° because this elevation is the most typical for data taking during normal operation. In Figure 9, the on-axis data is labeled center and exhibits the expected parabolic shape. The telescope is focused at Z_{mm}=37.8 ± 3.2 mm and r_{80} = 0.0463 ± 0.0024° based on the parabolic fit.

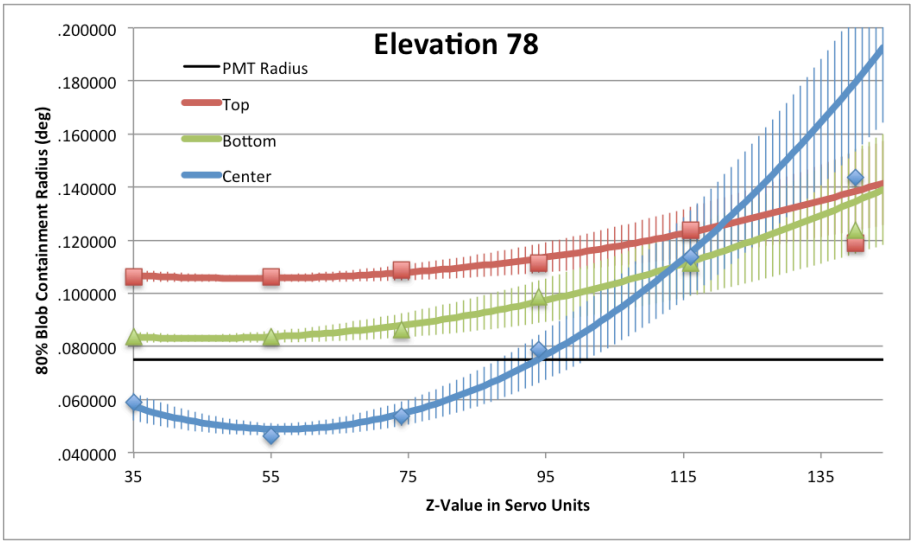

Figure 10 - r_{80} vs. Z_{SU} for Elevation 78°

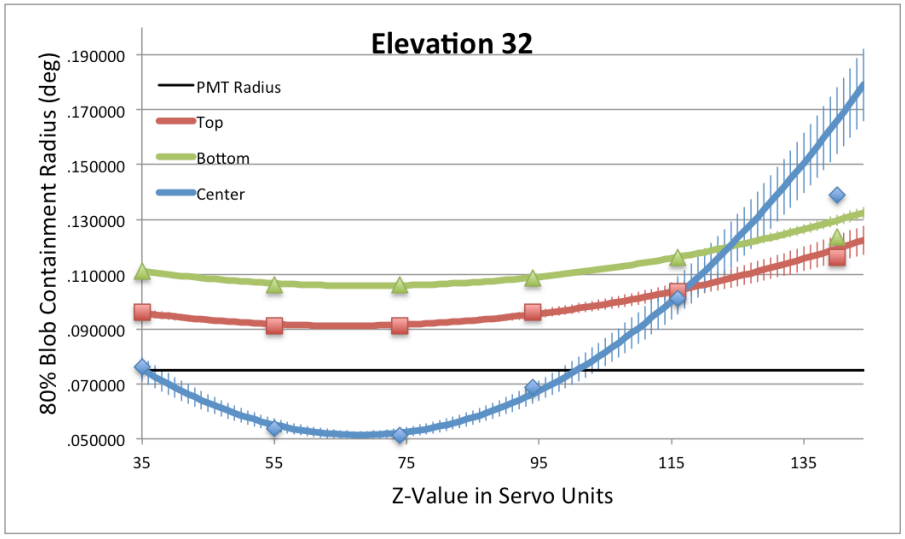

Figure 11 - r_{80} vs. Z_{SU} for Elevation 32°

We note that r_{80} is smaller than the black line at 0.075° which is the size of a PMT. The focus position is consistent with the front face of the light cones which are positioned at 43 mm. The off-axis focus is sharper for the bottom orientation than the top. The off-axis focus is generally larger than the size of a PMT. The Z_{mm} for off-axis is consistent with Z_{mm} at the center.

Next we examined elevation 78° and performed the same steps as above. In Figure 10 the output data from Plotpsf is shown as points and the graphical analysis fit lines are given for 78°. From the 78° data we draw similar conclusions as before. The telescope is focussed at Z_{mm}= 39.3 ± 2.3mm and r_{80} =0.0488 ± 0.0021° based on the parabolic fit. This focus is consistent with the 66° focus. Again, the off-axis focus is larger than the size of a PMT, while the on-axis is smaller.

The last elevation that was examined was 32°.

Orientation	Elevation	B (mm)	C (deg)
Center	32	47.1 ± 1.2	0.0514 ± 0.0015
Top	32	45.5 ± 1.7	0.0912 ± 0.0006
Bottom	32	47.6 ± 1.1	0.1058 ± 0.0003
Center	66	37.8 ± 3.2	0.0463 ± 0.0024
Top	66	33.5 ± 1.4	0.0956 ± 0.0002
Bottom	66	37.2 ± 2.7	0.0752 ± 0.0010
Center	78	39.3 ± 2.3	0.0488 ± 0.0021
Top	78	36.1 ± 5.2	0.1056 ± 0.0010
Bottom	78	31.5 ± 5.2	0.0830 ± 0.0012

Table 1 - Location (B) in mm and Size (C) in deg of the Minimums for each orientation and elevation

The telescope is focused at Z_{mm}= 47.1 ± 1.2 mm and r_{80} = 0.0514 ± 0.0015° based on the parabolic fit. This is in front of the face of the light cones. The focus is also not as sharp for both on-axis and off-axis data. Also, the bottom orientation for the elevation 32° was sharper than the top. This marked a decisive shift in the data.

The B and C values from Equation 3 fit to each orientation and elevation are organized in Table 1 for convenience and the PSF images are all collected in the Appendix, Figures 12-14. At elevations of 66° and 78° the minima are at 37.8 ± 3.2 mm and 39.3 ± 2.3 mm respectively. These are within one sigma of each other, however at an elevation of 32° the minimum shifted to 47.1 ± 1.2 mm.

There are two interesting take-away messages from the off-axis plots in in Figures 9, 10 and 11. The first is the relative size of r_{80} compared to the sizes of on-axis r_{80}. The off-axis r_{80} is typically larger than one PMT. At locations around the minimum they are nearly double the focused r_{80} size. The second is that for the two high elevations we see that r_{80} for the bottom orientation is sharper than the top orientation. At 32° we find the top orientation to be the sharper of the two. This result is not consistent with simple optical aberrations, which are symmetric. It would follow that the camera tends to favor some

middle elevation in which the top and bottom are equally focused.

Because the sharpest on-axis PSF occurs at a different location for this lower elevation and the top/bottom relative sizes flip we conclude that the telescopes undergo a structural sagging at low elevations.

6 - Conclusion

We conclude that the servo automation makes PSF characterization much easier and also produces more reliable data since measurements can be taken before sources move in the sky or the atmospheric conditions change. All of our data were taken in two hours and it significantly exceeded any other focal-plane experimentation done in the years of operation prior to summer 2011.

Our analysis shows that the 80% containment radius is a good measure of the PSF and focus properties of Telescope T4. The results provided the expected parabolic relationship between r_{80} and Z_{SU}. The r_{80} grew larger as the screen was moved in either direction away from the statistical minimum, as theory predicts.

The front face of the light cones is set at a position of 43 mm in Z_{mm}, which we compare to the location of the center minima for each elevation. For 66°, this location is 37.8 ± 3.2 mm which is 1.6σ from the light cone position. At elevation 78° the minimum was found at 39.3 ± 2.3 mm also resulting in a 1.6σ difference. Within our uncertainty we find that the focal point is consistent with the location of the front of the light cones. Elevation 32° had the large shift in on-axis minimum location to 47.1 ± 1.2 mm. This shift results in a 4.1 mm (3.4σ) distance between the focal plane and the light cones. At the front face of the light cones we find that r_{80} is still smaller than the size of a PMT with a radius of 0.052 ± 0.005°. Also, this is the only elevation where the focal plane is higher than the light cone extension.

From our data we conclude that the light cones were placed properly for normal data taking at higher elevations, but may experience issues at lower elevations like 32°.

Although the on-axis PSFs are smaller than the size of a PMT in the camera, the off-axis PSFs are generally larger. The 80% blob containment off-axis was always larger than the size of the on-axis blob. Because of this, care must be taken in the science analysis of VERITAS data. These measurements have been passed to the simulation group to aid in modeling the VERITAS performance accurately.

There are two aspects of the data that indicate a structural sagging. First, we found that elevation has a discernible effect on B in Equation 3. B is the location of the minimum of the fitted parabola, and is the measured focal point. The focused image distance is shorter for elevation 32° than for the two higher elevations. This needs to be considered when analyzing low elevation data collected by VERITAS. Second, the off-axis r_{80} values also show that elevation 32° is different from the higher elevations. For the higher elevations, the bottom off-axis image is more focused than the top. The converse is true for elevation 32°. These two effects lead us to believe that one of two types of sagging occur; either the support that holds mirrors warped under stress or the camera box itself sags.

As with most early forms of experiments, the key to better understanding is more data and more kinds of data. Future measurements will adopt a smaller step size in image distance for more accuracy and a smaller offset for off-axis measurements. We also look forward to making similar measurements of the other 3 telescopes on site.

7 – Appendix: PSF Images

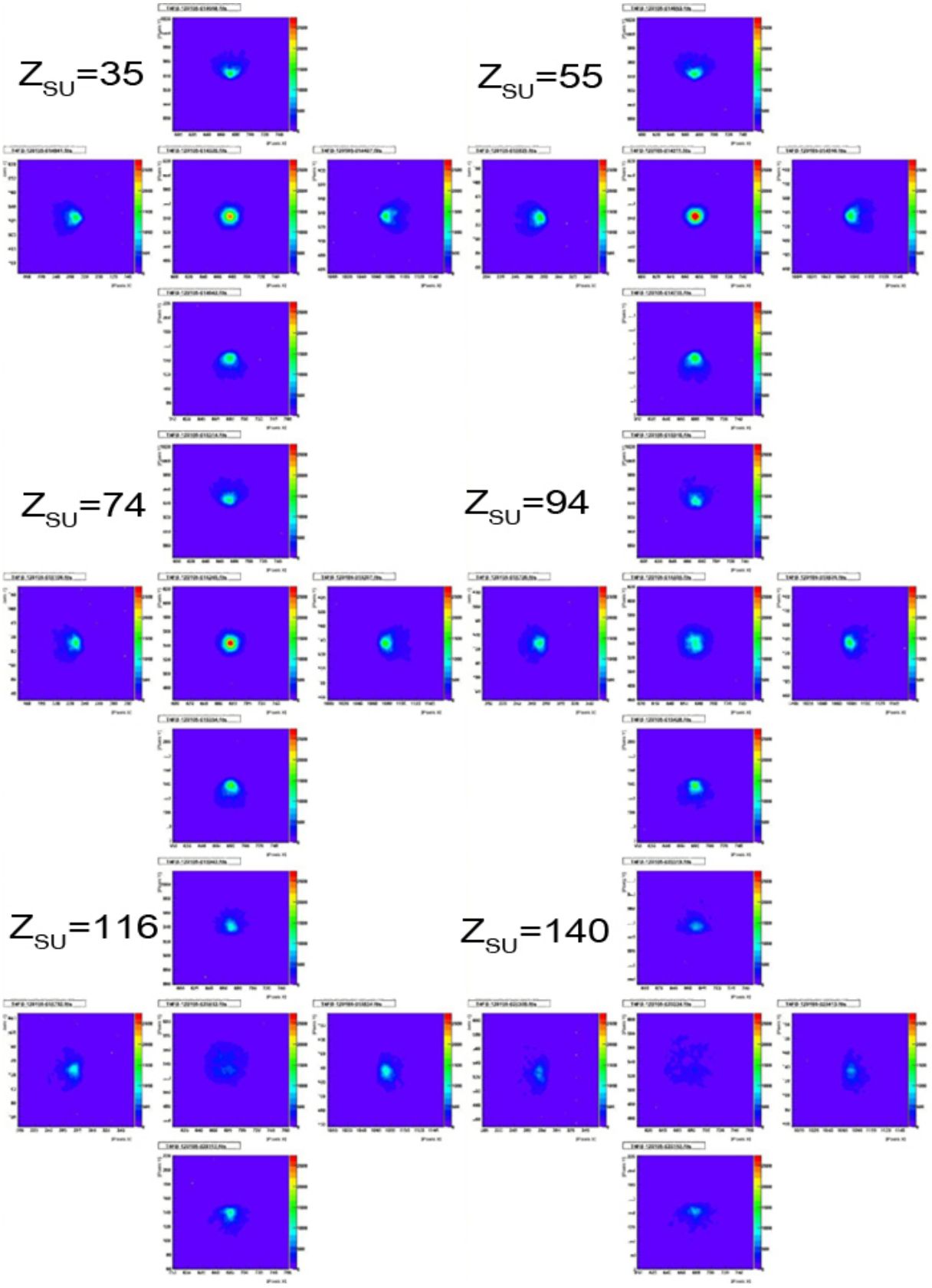

Figure 12 - The Plus-Shaped Grid for Each SU Value at 66°

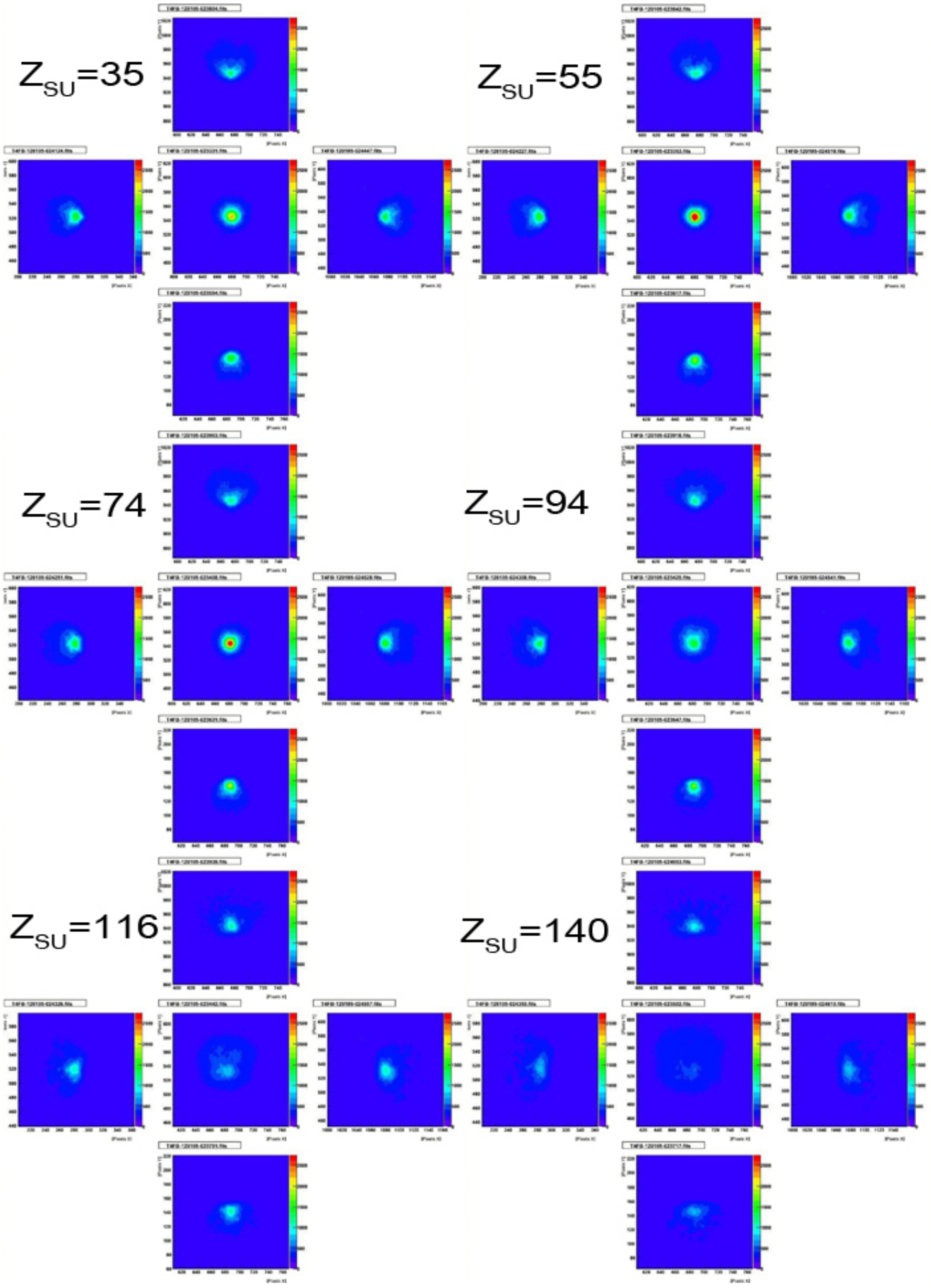

Figure 13 - The Plus-Shaped Grid for Each SU Value at 78°

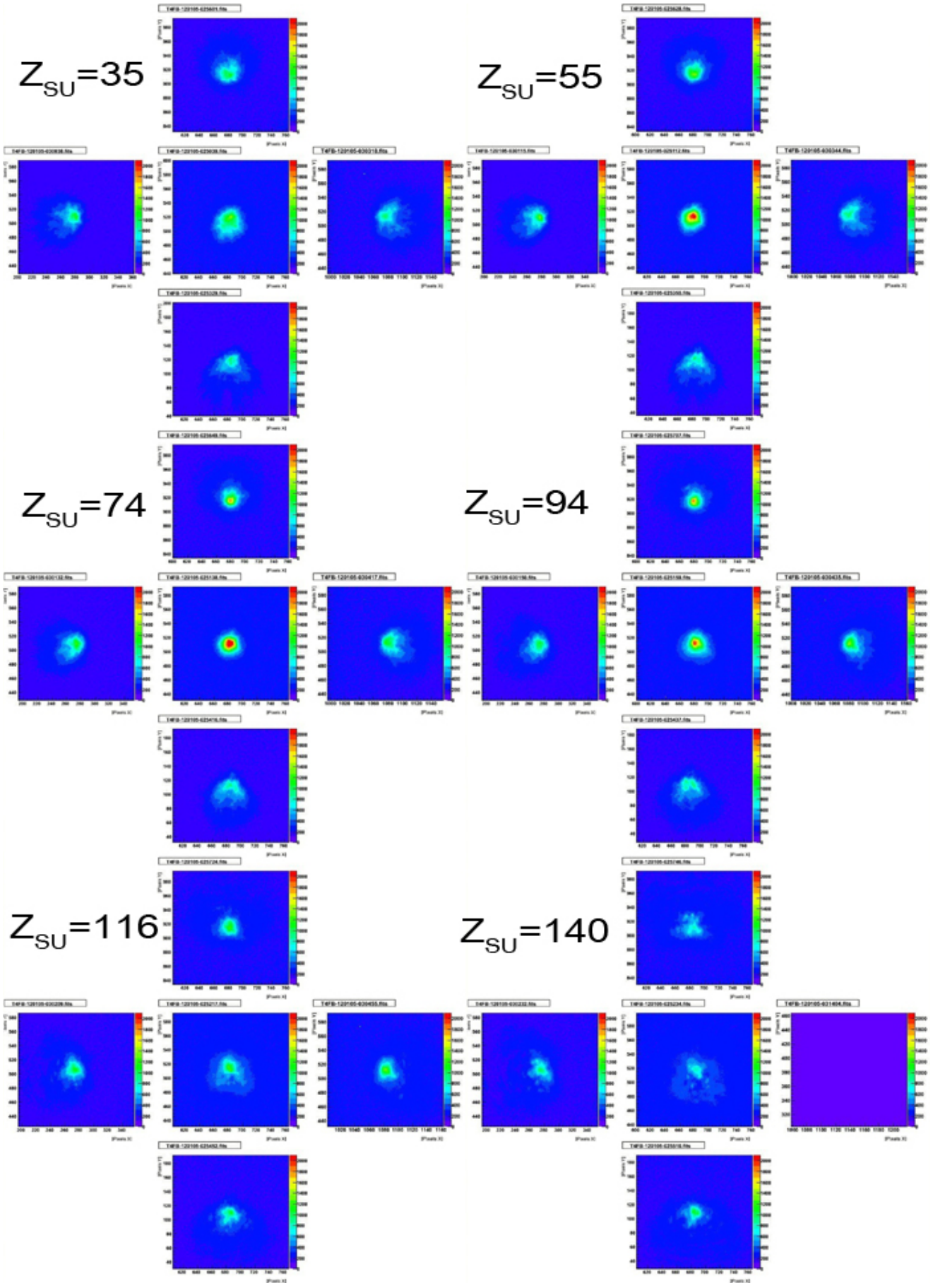

Figure 14 - The Plus-Shaped Grid for Each SU Value at 32°